

High Temperature Deformation Mechanism Maps for γ -TiAl Based-alloys with DP/NG Structures: Construction and Application

Cheng Liang¹, Chen Yi^{1,2}, Xue Xiangyi³, Kou Hongchao³, Li Jinshan³, Bouzy Emmanuel^{4,5}

¹ Jiangsu University of Technology, Changzhou 213001, China; ² Sunnywell (China) New Material Technology Co., Ltd, Changzhou 213000, China; ³ State Key Laboratory of Solidification Processing, Northwestern Polytechnical University, Xi'an 710072, China; ⁴ LEM3, CNRS UMR 7239, Université de Lorraine, Ile du Saulcy, 57045 Metz Cedex 1, France; ⁵ DAMAS, Université de Lorraine, Ile du Saulcy, 57045 Metz Cedex 1, France

Abstract: Once the metallic materials are subject to stress, a number of independent or alternative mechanisms may initiate and contribute to deformation. As for the γ -TiAl-based alloys whose deformation kinetics is fairly complex, it is of particular significance to quantify the general constitutive relationship produced by each possible mechanism and to identify the predominant mechanism at any specific loading conditions. For this purpose, in the present study Ashby-type deformation mechanism maps concerning six major deformation mechanisms were constructed for various TiAl alloys with duplex (DP) and near-gamma (NG) microstructures. The general features as well as the effect of grain size on the appearance of the maps were analyzed. After a detailed discussion, it is believed that the proposed deformation mechanism maps are powerful tools in understanding the deformation mechanisms and predicting the deformation kinetics of DP/NG-TiAl alloys. In particular, they are demonstrated to be useful reference in alloy design and determination of proper processing parameters.

Key words: TiAl alloys; deformation mechanism; deformation kinetics; dislocation creep; grain boundary sliding; diffusion creep

It is well-known that when a crystal is subject to an external stress, a number of independent or alternative deformation mechanisms can initiate and contribute to the total strain rate. The one which provides the highest strain rate is thought to be rate-controlling. Then a rate-equation (or constitutive model) is essential for each rate-controlling process. Deformation mechanism map (DMM) is an approach that allows to quantitatively express the complex constitutive equations and at the same time allows to visualize the physical concepts about the mechanisms involved^[1,2]. DMM was firstly proposed by Ashby and Frost^[1,3], which was developed on the concept of “creep diagram” suggested by Weertman^[4]. Till date, DMM has been widely used and some new forms have

been proposed^[5,6]. As for the TiAl alloys, Hayes and Martin^[7] have made the first attempt to construct the DMM for a Ti-53Al-1Nb alloy on the basis of experimental observation. Gorzel and Sauthoff^[8] have developed DMMs for Ti-55Al and Ti-51Al alloys based on experimental results and theoretical rate-equations. Note that these DMMs are specifically developed for certain TiAl alloys and focused on limited rate-controlling processes (only two deformation mechanisms, dislocation creep and Coble creep, have been concerned). Hence the reusability of these DMMs for other TiAl alloys is poor.

Obviously, the attempt to construct universal DMMs for TiAl alloy-system requires a comprehensive understanding

Received date: November 27, 2018

Foundation item: National Natural Science Foundation of Jiangsu Province (BK20160291); the Natural Science Foundation of the Jiangsu Higher Education Institutions (17KJB430013); the fund of the State Key Laboratory of Solidification Processing in NWPU (SKLSP201822); the Fund of the Jiangsu Planned Projects for Postdoctoral Research Funds (1701006B)

Corresponding author: Cheng Liang, Ph. D., School of Materials and Engineering, Jiangsu University of Technology, Changzhou 213001, P. R. China, Tel: 0086-519-86953289, E-mail: chengliang525@163.com

Copyright © 2019, Northwest Institute for Nonferrous Metal Research. Published by Science Press. All rights reserved.

of the general deformation mechanisms at any loading conditions and essentially, a series of unified rate-equations. A critical prerequisite is to identify the major limiting factors affecting the deformation behaviour. Zhang and Deevi^[9] have investigated the limiting factors of the creep rate for various TiAl alloys from 40 previous studies. They found that for TiAl alloys with full-lamellar or near-lamellar microstructures, the creep rate was affected by many factors such as lamellar spacing, additions of W, C, N, or Si, etc. In contrast, γ grain size is the sole (major) limiting factor for those with duplex (DP) or near-gamma (NG) microstructures. Moreover, in a previous review^[10], we have analyzed the mechanical data of various DP/NG-TiAl alloys published in the last twenty years, and also noted that their high temperature deformation kinetics is mainly controlled by the lattice or grain boundary diffusivity, with γ grain size as the major limiting factor. Correspondingly, six specific deformation mechanisms were identified and a group of unified rate-equations have been developed. These rate-equations provide an excellent opportunity to construct the universal DMMs for DP/NG-TiAl alloys. Hence in this study, a series of DMMs have been constructed and analyzed based on these rate-equations. Their importance in alloy design, wrought processing and deformation mechanism prediction was discussed.

1 Rate-equations and Calculation Procedures

Table 1 tabulates the rate-equations quoted from Ref.[10] for various high temperature deformation mechanisms of DP/NG-TiAl alloys. Six rate-controlling processes were identified, namely, power-law creep (PL), power-law breakdown (PLB), lattice diffusion-controlled grain boundary sliding (D_L -GBS), grain boundary diffusion-controlled grain boundary sliding (D_B -GBS), lattice diffusion creep (Nabarro-Herring creep, N-H), and grain boundary diffusion

creep (Coble creep, Coble). Among them, PL and PLB are alternative mechanisms involving the same crystalline defects^[1]. All the other mechanisms are independent that can simultaneously contribute to the total deformation. It should be stressed that although GBS or diffusion creep requires accommodation processes such as dislocation creep, these accommodation processes themselves cannot contribute to the macroscale creep rate^[10]. Once the DP/NG-TiAl alloys were subject to applied stress, to a first approximation, the total strain rate can be calculated by^[11]:

$$\dot{\epsilon}_{\text{Total}} = (\dot{\epsilon}_{\text{PLB}} \text{ or } \dot{\epsilon}_{\text{PL}}) + (\dot{\epsilon}_{D_L\text{-GBS}} + \dot{\epsilon}_{D_B\text{-GBS}}) + (\dot{\epsilon}_{\text{N-H}} + \dot{\epsilon}_{\text{Coble}}) \quad (7)$$

The applied thermo-physical parameters for TiAl alloys are listed in Table 2, where the elastic properties and diffusion coefficient were quoted from Ref. [11] and [12], respectively. Matlab software was applied to compute the Ashby-type DMMs, namely, the vertical axis of the map represents the normalized equivalent stress, σ/G , and the horizontal axis denotes the homologous temperature, T/T_m ^[11]. The applied calculating programme is as follows. Firstly, the temperature/stress space was meshed into 1000×1000 nodes. For each node the six strain rate values were calculated by rate-equations tabulated in Table 1. Secondly, at each temperature-stress node, the mechanism which produced the highest strain rate was identified as the rate-controlling process at such a condition. The boundaries between any adjacent mechanism fields were outlined. Finally, the total strain rate for each node was calculated using Eq.(1) and the contours were superimposed on the maps.

2 Results and Discussion

2.1 General features

A computed DMM for DP/NG-TiAl alloys with a typical γ grain size of 30 μm is shown in Fig.1. Note that the blue

Table 1 Rate-equations of various deformation mechanisms for DP/NG-TiAl alloys^[10]

Deformation mechanism	Rate-equation	Number
Power-law breakdown (PLB)	$\frac{\dot{\epsilon}kT}{GbD_L} = 8 \times 10^{-3} \left[\sinh \left(160 \frac{\sigma}{G} \right) \right]^4 \left(\frac{d}{b} \right)^{-1}$	(1)
Power-law creep (PL)	$\frac{\dot{\epsilon}kT}{GbD_L} = 5 \times 10^{-6} \left(\frac{\sigma}{G} \right)^4 \left(\frac{d}{b} \right)^{-1}$	(2)
Lattice diffusion- controlled grain boundary sliding (D_L -GBS)	$\frac{\dot{\epsilon}kT}{GbD_L} = 1 \times 10^6 \left(\frac{\sigma}{G} \right)^2 \left(\frac{d}{b} \right)^{-2}$	(3)
Grain boundary diffusion-controlled grain boundary sliding (D_B -GBS)	$\frac{\dot{\epsilon}kT}{G\delta D_{GB}} = 3 \times 10^2 \left(\frac{\sigma}{G} \right)^2 \left(\frac{d}{b} \right)^{-3}$	(4)
Nabarro-Herring creep (N-H creep)	$\frac{\dot{\epsilon}kT}{GbD_L} = 10 \left(\frac{\sigma}{G} \right) \left(\frac{d}{b} \right)^{-2}$	(5)
Coble creep	$\frac{\dot{\epsilon}kT}{G\delta D_B} = 30 \left(\frac{\sigma}{G} \right) \left(\frac{d}{b} \right)^{-3}$	(6)

line denotes where the eutectoid reaction occurs. The predicted strain rate contours from 10^{-10} s^{-1} to 10^1 s^{-1} are plotted as black thin curves. It should be pointed out that because the accuracy of the rate-equations is questionable at ultra-high temperatures^[10], the strain rate contours are represented by dotted line above the eutectoid reaction. From the inspection of the plot one can conclude the general features of DMMs for DP/NG-TiAl alloys:

(1) Coble field occupies most area of the map due to the absence of the threshold stress in the rate-equations^[10]. One can assume that if the alloy is subject to a stress lower than yield strength at ambient temperature, elastic deformation immediately occur but will be ultimately replaced by permanent plastic deformation via Coble creep. However, the strain rates in this field are generally quite low that even cannot be detected by experimental equipments.

(2) N-H creep only controls the deformation at ultra-high

temperatures (near the melting point) under significantly low stresses. Such a temperature-stress range is far beyond the interests of investigators. This may be the reason why there has been no report about N-H creep in TiAl alloys till date.

(3) At stress level higher than that for N-H creep, D_L -GBS starts to be predominant and covers an appreciably large field. Because the alloys generally exhibit superplasticity when GBS is the major deformation mechanism, the enlarged GBS field confirms that DP/NG alloys are suitable for processing.

(4) Further increase of the stress leads to the appearance of PL field. Surprisingly, the PL creep field is fairly small and locates in quite high stress level. From this viewpoint, the lack of stable PL creep regime of TiAl alloys (the stress exponents are scattered and generally increased with the increase of applied stress^[13]) may be clarified. As summa-

Table 2 Thermo-physical parameters of TiAl-based alloys

Parameters	Values	
Crystallographic and thermal data		
Burgers vector, b/m	2.83×10^{-10}	
Atomic volume, Ω/m^3	1.59×10^{-29}	Estimated by $\Omega=0.7b^3$
Melting point, T_m/K	1780	An average value
Eutectoid transus, T_e	$0.8T_m$	An average value
Shear modulus, G		
Shear modulus at 0 K, G_0/GPa	74.24	
Temperature dependence, $dG/dT/GPa \cdot K^{-1}$	0.0141	Quoted from [11]
Lattice diffusion coefficient, D_L		
Pre-exponential, $D_{0L}/m^2 \cdot s^{-1}$	0.0211	
Activation energy, $Q_L/kJ \cdot mol^{-1}$	360	Quoted from [12]
Grain boundary diffusion coefficient, D_B		
Pre-exponential, $\delta D_{0B}/m^3 \cdot s^{-1}$	6×10^{-12}	Estimated by $\delta D_{0B}=bD_{0L}$
Activation energy, $Q_B/kJ \cdot mol^{-1}$	215	Estimated by $Q_B=0.6Q_L$

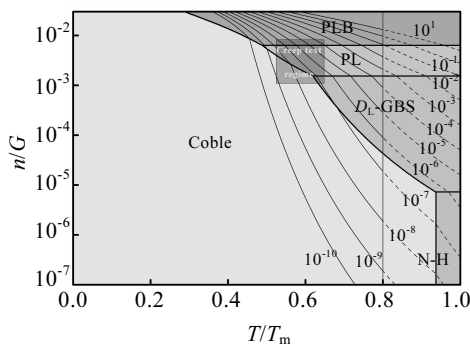


Fig.1 Calculated DMM for DP/NG-TiAl alloys with a typical grain size of $30 \mu\text{m}$ (the blue line represent where the eutectoid reaction occurs. The rectangular shadow represents the general parameter regime for dislocation creep tests)

rized by Ref.[13], most of the creep tests were performed in the temperature range of $676 \sim 877 \text{ }^\circ\text{C}$ (i.e., $0.53 T_m \sim 0.65 T_m$) with a stress range of $80 \sim 500 \text{ MPa}$ (i.e., $0.001G \sim 0.008G$). If we superimpose such a range on the map, as indicated by the blue shade in Fig.1, one can note this region partially overlaps PL and Coble fields, and even extends into the PLB and GBS fields. That is, the predominant deformation mechanism is mutable at such loading conditions, which leads to unstable deformation kinetics.

(5) At stresses higher than $0.0065G$, PLB occurs. However, its upper boundary cannot be established due to the lack of the rate-equation for thermo-activated dislocation glide.

2.2 Grain size effect

The rate-equations shown in Table 1 indicate that the grain size (d) is always the most important factor affecting

the deformation kinetics. Because the grain size exponents of these mechanisms are not identical, the variation of grain size can definitely result in the swelling or shrinkage of some fields. Fig.2a~2f show a series of maps with different grain sizes (from 0.1 to 100 μm), which clearly reveals the effect of grain size on the DMMs.

(1) When the alloys have a submicrocrystalline grain size (Fig.2a), Coble creep dominates nearly all of the temperature-stress space of the map. Only in the ultra-high temperature and stress range (upper-right corner of the map) can the PLB and D_L -GBS occur. With the increasing grain size up to 1 μm (Fig.2b), the PLB and D_L -GBS fields gradually expand toward lower stresses and temperatures at the expense of Coble field. As expectation, N-H creep and PL creep fields have not emerged due to the small grain size. Meanwhile, it is curious that the DB-GBS mechanism is also suppressed. This is contradictory to the common views that DB-GBS is the rate-controlling process in submicrocrystalline TiAl alloys at superplastic conditions^[14,15]. Probably this is because, as observed by Imayev et al^[15],

dramatic strain-induced grain growth occurs when the submicrocrystalline TiAl alloys were subject to superplastic tension. For instance, the initial grain size of a Ti-46Al alloy was about 0.2 μm , and after superplastic deformation at 900 $^\circ\text{C}$ it increased up to about 2 μm which is almost ten times larger than that of the initial state. According to Eq.(4) in Table 1, we can note that such a coarsening of grain size leads to the deceleration of the superplastic creep kinetics by a factor of 10^3 . That is, to a first approximation, the practical strain rate would be 10^3 times higher than that predicted by Eq.(4), because the parameter d in the rate-equations denotes the initial grain size.

(2) Increase of the grain size up to micron level (Fig.2c) leads to the presence of the PL field between PLB and D_L -GBS fields. Although in such a case the PL field only occupies a very narrow stress range, it significantly affects the appearance of the maps. On the one hand, it determines the lower boundary (0.0065G which is independent on grain size) of PLB field. On the other hand, it pushes the D_L -GBS field downward to lower stress level. Meanwhile, with fur-

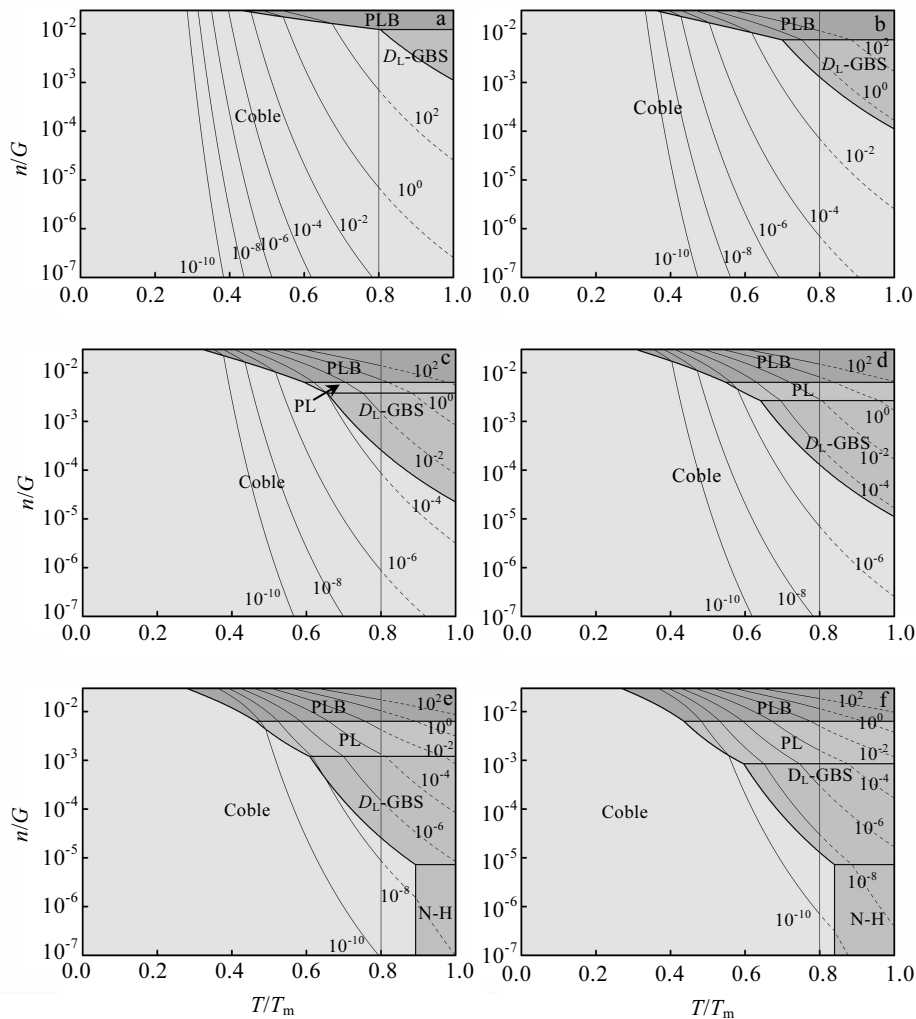


Fig.2 Effect of grain size on the DMMs for DP/NG-TiAl alloys: (a) 0.1 μm , (b) 1 μm , (c) 5 μm , (d) 10 μm , (e) 50 μm , and (f) 100 μm

ther the increase of grain size (Fig.2d), all the three fields (PLB, PL and D_L -GBS) continue to expand toward low temperatures, accompanied with the continuous shrinkage of the Coble field. Meanwhile, the PL and D_L -GBS field also expands toward the lower stresses.

(3) When the grain size increases up to 50 μm (Fig.2e), N-H field appears in the lower-right corner of the maps. The boundary between N-H and D_L -GBS fields is at the stress level of about $10^5 G$ and is independent on grain size due to the same grain size exponent (see Eq.(3) and Eq.(5) in Table 1) of these two mechanisms. It should be noted that the presence of the N-H field immediately stops the expansion of the GBS field toward lower stresses, but meanwhile the D_L -GBS field is continuously compressed by the enlarging PL field. Consequently, although the GBS/Coble field boundary simultaneously moves forward to the low temperatures with the increasing grain size (Fig.2f), the area of D_L -GBS field actually shrinks (compare Fig.2e with Fig.2f). One can readily speculate that if the rate-equations are still valid when the grain size is sufficiently large, the D_L -GBS field would disappear and be replaced by PL field eventually.

(4) Another distinct phenomenon is the evolution of strain rate contours. With the increase of grain size, the contours notably shift toward the upper-right corner of the maps, i.e., higher temperatures and higher stresses. This is in accordance with expectation because the deformation resistance is increased with the increase of grain size at ele-

vated temperatures.

2.3 Comparison with ordinary alloys

Until now a number of DMMs have been developed for various crystals. If the materials have the same microstructural features, the difference between their DMMs is dependent on their crystallography and the nature of the bonds holding their atoms together^[1]. Therefore, the DMMs of TiAl alloys may exhibit some unique features in comparison with normal disordered metallic materials.

Three alloys, i.e., pure aluminium, Ti-10Al and MAR-M200 have been selected for comparison. Note that the first two alloys can be regarded as the constituents for TiAl alloys and the third is a typical Ni-based superalloy for high temperature use. All the maps for these three alloys have been recalculated by the rate-equations proposed by Ref.[1] and Ref. [16]. To make the comparison more intuitive, several considerations have been taken into account: (1) All maps refer to a standard microstructure state so that the grain size of all the alloys were set to be 30 μm . (2) Only three mechanisms (PL, Coble and N-H creep) have been concerned. (3) The strain rate contours shown on the maps are from 10^{-10} ~ 10^0 s^{-1} . If the strain rate is lower than 10^{-10} s^{-1} , it is too slow to be detected so that only elastic deformation is thought to occur (Ashby and Frost^[1,3] have adopted 10^{-8} s^{-1}). Then a large field of the maps is replaced by purely elastic deformation, as indicated in Fig.3.

According to the maps shown in Fig.3, it is found that in comparison with ordinary metallic materials such as pure Al

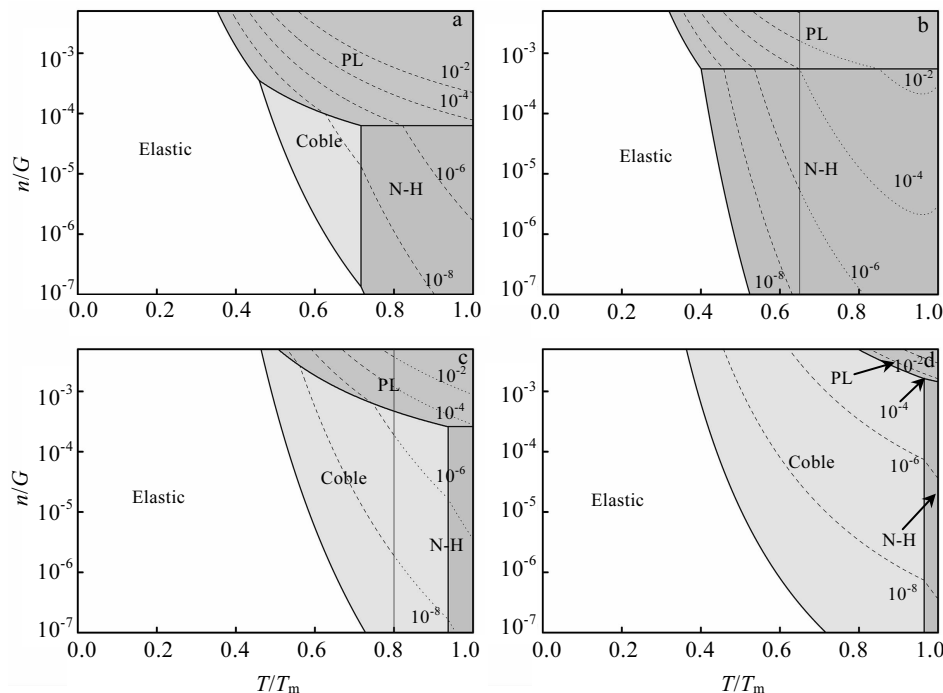


Fig.3 Calculated DMMs for various alloys with a same grain size of 30 μm : (a) pure Al; (b) Ti-10Al alloy; (c) TiAl alloy; (d) MAR-M200 superalloy (note that for Ti-10Al alloy, the map is constructed only using the thermo-physical parameters of α phase; the $\alpha \rightarrow \beta$ transus is indicated by blue line on the map)

metal (Fig.3a) and Ti-10Al alloy (Fig.3b), the most pronounced feature of the DMM (Fig.3c) for TiAl alloy is that it is more susceptible to Coble creep. This reduces the N-H area and pushes the transition temperature which separates them to higher temperatures. In contrast, the Coble fields for ordinary alloys are quite small (Fig.3a for Al) and even disappear (Fig.3b for Ti-10Al). Instead, they have particularly large N-H field. Meanwhile, the PL field of TiAl alloys also shrinks significantly in comparison with those for Al and Ti-10Al alloys. This is because the PL creep is dramatically retarded in TiAl alloys, which have been already discussed in Ref.[10]. The strain rate contours confirm the lower PL creep rates in TiAl alloys than in ordinary metallic materials. Consequently, the Coble creep field swells and expands to higher stress level.

The DMM of MAR-M200 alloy has similar features with those of TiAl alloys. As shown in Fig.3d, the MAR-M200 alloy is also characterized by an enlarged Coble field but small PL/N-H fields. Moreover, in comparison with TiAl alloys, this feature is more prominent probably due to its superior high temperature performance (can be clearly revealed by the strain rate contours). Therefore, one may conclude that the TiAl alloys behave much more like Ni-based superalloys rather than their solid solution forms (Ti or Al disordered alloys). Given this conclusion, one may further speculate that the DMMs of high temperature alloys must have small N-H and PL fields and an enlarged Coble field, which can be considered as the prerequisites for high temperature alloys. From this perspective, the proposed DMMs are useful tools for the alloy design.

2.4 Case study

Since DMMs can clearly and quantitatively indicate strain rate contours in each region where specific deformation mechanism is predominant, they provide a strong predictive tool that can be used to estimate one of three variables (strain rate, stress and temperatures) if the other two have been determined. In general, determination of the strain rate and temperature range for a specific deformation mechanism is not ready. It requires systematic experimental tests which are time-consuming and high-cost. However, by the present DMM, this process (identify the proper parameters) is significantly simplified. For instance, there is a TiAl alloy workpiece with a grain size of $\sim 5 \mu\text{m}$, it is wondered what is the proper strain rate range for superplastic deformation at $1000 \text{ }^\circ\text{C}$. From the corresponding DMM shown in Fig.2c, it is clearly manifested that $10^{-4}\sim 10^{-3} \text{ s}^{-1}$ roughly fulfills the requirement. Experimental verification confirms that at $1000 \text{ }^\circ\text{C}/2\times 10^{-4} \text{ s}^{-1}$, the Ti-43.5Al- 8Nb-0.2W alloy with $\sim 5 \mu\text{m}$ grain size exhibits notable superplasticity, as demonstrated by Fig.4.



Fig.4 Tensile specimens of Ti-43.5Al-8Nb-0.2W alloy with a grain size of $\sim 5 \mu\text{m}$ before and after tension at $1000 \text{ }^\circ\text{C}/2\times 10^{-4} \text{ s}^{-1}$ (note that glass lubricant was applied to protect the surface oxidation during tension)

3 Conclusions

1) The proposed DMMs for various TiAl alloys with DP/NG microstructures are powerful tools in quantifying the deformation kinetics and prediction of deformation mechanisms. Moreover, they are demonstrated to be useful reference in alloy design and determination of proper processing parameters

2) The DMMs of DP/NG-TiAl alloys are characterized by large Coble field and D_L -GBS field, whereas the PL creep field and N-H creep field are quite small. This feature is more like those of superalloys, rather than those for their solid solution forms (Ti or Al disordered alloys). Moreover, the small PL field partially explains why there is no stable power-law creep regime for TiAl alloys. However, the D_B -GBS field does not emerge on the maps due to the underestimation of the D_B -GBS rate. The morphology of the DMMs is sensitive to the grain size. When the grain size is very small, only Coble, PLB and D_L -GBS fields can be identified. With the grain size increasing, other mechanism fields such as PL and N-H creep gradually appeared, and all these fields enlarge at the expense of Coble creep field. Meanwhile, when the grain size is sufficiently large, the D_L -GBS field begins to shrink.

References

- 1 Frost H J, Ashby M F. *Deformation Mechanism Maps: the Plasticity and Creep of Metals and Ceramics*[M]. Oxford: Pergamon Press, 1982: 1
- 2 Notis M R. In Bradt R C, Tressler R E eds. *Deformation of Ceramic Materials*[M]. Pennsylvania: Springer, 1975: 1
- 3 Ashby M F. *Acta Metallurgica*[J], 1972, 20: 887
- 4 Weertman J. *Transactions ASM*[J], 1968, 61: 681
- 5 Dahlberg C F O, Faleskog J, Niordson C F et al. *International Journal of Plasticity*[J], 2013, 43: 177
- 6 Yamakov V, Wolf D, Phillpot S R et al. *Nature Materials*[J],

- 2004, 3(43-47): 43
- 7 Hayes R W, Martin P L. *Acta Metallurgica et Materialia*[J], 1992, 40: 2167
- 8 Gorzel A, Sauthoff G. *Intermetallics*[J], 1999, 7(3-4): 371
- 9 Zhang W, Deevi S. *Materials Science and Engineering A*[J], 2003, 362: 280
- 10 Cheng L, Li J S, Xue X Y et al. *Materials Science and Engineering A*[J], 2016, 678: 389
- 11 Schafrik R E. *Metallurgical Transactions A*[J], 1977, 8(6): 1003
- 12 Mishin Y, Herzig C. *Acta Materialia*[J], 2000, 48: 589
- 13 Kassner M E. *Fundamentals of Creep in Metals and Alloys*[M]. London: Butterworth-Heinemann, 2015
- 14 Sun J, He Y H, Wu J S. *Materials Science and Engineering A*[J], 2002, 329-331: 885
- 15 Imayev R M, Salishchev G A, Senkov O N et al. *Materials Science and Engineering A*[J], 2001, 300: 263
- 16 Janghorban K, Esmaeili S. *Journal of Materials Science*[J], 1991, 26: 3362

双态/近 γ 组织 TiAl 合金的变形机制图谱：构建及应用

程亮¹, 陈逸^{1,2}, 薛祥义³, 寇宏超³, 李金山³, Bouzy Emmanuel^{4,5}

(1. 江苏理工学院, 江苏 常州 213001)

(2. 盛利维尔(中国)新材料技术有限公司, 江苏 常州 213000)

(3. 西北工业大学 凝固技术国家重点实验室, 陕西 西安 710072)

(4. LEM3, CNRS UMR 7239, Université de Lorraine, Ile du Saulcy, 57045 Metz Cedex 1, France)

(5. DAMAS, Université de Lorraine, Ile du Saulcy, 57045 Metz Cedex 1, France)

摘要: 当金属材料承受应力时, 某些独立或非独立的变形机制可同时被激活。对于变形动力学极其复杂的 γ -TiAl 基合金, 定量描述每个变形机制的一般性本构行为、预测指定加载条件下的主要变形机制具有重要的科学和实际意义。为此, 本研究针对具有双态/近 γ 组织的 TiAl 合金, 构建了同时考虑 6 种机制的变形机制图谱, 并详细分析了其形貌特征, 探讨了晶粒度的影响。研究表明, 本研究所提出的变形机制图谱是理解 TiAl 合金变形机制、预测变形动力学的有力工具。特别是该变形机制图谱可为 TiAl 合金设计及变形工艺制定提供重要借鉴。

关键词: TiAl 合金; 变形机制; 变形动力学; 位错蠕变; 晶界滑动; 扩散蠕变

作者简介: 程亮, 男, 1988 年生, 博士, 讲师, 江苏理工学院材料工程学院, 江苏 常州 213001, 电话: 0519-86953289, E-mail: chengliang525@163.com